Manuscript refereed by Professor Monika Willert Porada, Bayreuth University

Synthesis, Characterization and FEM-simulation of W/CuCrZr-Composites for Extreme Thermal Applications

S. Nawka[a], T. Schubert[b], A. Brendel[c], A. Zivelonghi[c], J.-H. You[c], B. Kieback[a,b]

[a] *Institut für Werkstoffwissenschaft, Technische Universität Dresden, D-01062 Dresden, Germany*
[b] *Fraunhofer-Institut für Fertigungstechnik und Angewandte Materialforschung, Institutsteil Dresden, Winterbergstr. 28, D-01277 Dresden, Germany*
[c] *Max-Planck-Institut für Plasmaphysik, Boltzmannstr. 2, D-85748 Garching, Germany*

Abstract

Plasma facing components in fusion devices have to withstand extreme thermal loads. To fulfil the desired requirements we investigate tungsten as a plasma facing and CuCrZr as a heat sink material. However, the challenge is the big difference in their coefficients of thermal expansion (CTE). To reduce the thermally induced stresses, we utilize functionally graded materials (W/CuCrZr) as an interlayer between pure W and CuCrZr. In our work the optimized gradient structure will be constructed by means of FEM-simulation of stress-strain curves, CTE- and thermal conductivity values. The simulations are based on photorealistic input from SEM-cross sections of homogeneous W/CuCrZr-composites. The composites (30 to 70 vol.% CuCrZr) were fabricated by pressing of a W-powder / space-holder mixture, debinding/sintering, CuCrZr-infiltration and heat treatment. The measured properties fit quite well with simulated data. Furthermore, the mechanical properties are much better than with pure Cu. First examples of gradient structures will be shown.

Introduction

W/Cu-composites are applied in electronic devices (heat sinks) and energy systems (contact material in power switches). Beside this, they are of special interest as part of plasma facing components (PFCs) in future fusion devices [1-3]. In these cases PFCs are comprised of pure tungsten as a plasma facing material and pure Cu as a heat sink material. Tungsten is used especially because of its high temperature resistance and low sputter yield during plasma load whereas Cu is applied due to its very good thermal conductivity. In order to meet the challenge of the big difference in their coefficients of thermal expansion (CTE) and consequently lower the thermally induced stresses, a functionally graded W/Cu-composite is utilized as an interlayer between pure W and Cu [1-3].
W/Cu functionally graded materials (FGMs) are often fabricated by powder metallurgical processes [4,5] whereas plasma spraying is also possible [6]. The most popular way to produce W/Cu FGMs is by forming a tungsten skeleton with graded open pores and subsequent copper infiltration [1,2,7,8]. For the preparation of a graded tungsten skeleton several kinds of methods such as by using different particle size W powders [1,2], space holders [2], centrifugal powder forming (CPF) [7], electrochemical gradation [8] and powder segregation [9] were developed. The optimal thermal conductivity of the W/Cu FGM is achieved by creating a penetration microstructure where a continuous Cu network is present [10]. Further important properties are a homogeneous phase distribution and a low residual porosity.
To analyze the stress in the micro range and calculate the strain profile in the macro range of the W/Cu FGMs a couple of FEM simulations [1,6,11-13] and neutron diffraction measurements were performed [11,12]. They show that it is possible to optimize the gradient structure by varying composition and size.

As a novel approach in this work precipitation hardened CuCrZr is used instead of pure Cu because of its higher strength [14]. For FEM calculations an advanced simulation procedure called direct mapping FEM is applied [15]. This technique combines real microstructural data with fundamental material data as a basis for understanding the material behaviour. To validate the simulation results the calculated data on homogeneous W/Cu composites (stress-strain curves, thermal conductivity) is correlated to the measured experimental data. Furthermore first W/CuCrZr gradient structures were prepared.

Experimental

The production of W/CuCrZr-composites was based on two steps. First of all a porous tungsten skeleton with a defined open porosity, narrow pore size distribution as well as small difference in W-particle and pore size was formed. The starting materials were a tungsten powder with a d_{50}-value of 4μm from Plansee Metall, Austria and the amid wax ethylene bisstearamide from Hoechst, Germany as a space holder. The amid wax had a slightly higher d_{50}-value of ~12μm.
The tungsten powder and the amid wax were mixed together and ground in a mortar for ~30min to increase the homogeneity. Next, green compacts were uniaxially pressed at different pressures and debinded/sintered in hydrogen at 450°C for 30min and 1200°C for 60min respectively. For the production of a porous graded tungsten skeleton with three layers the mixed powders were pressed layer by layer and then debinded/sintered.
In the second step CuCrZr sheets (Elmedur X; Thyssen Duro Metall, Germany) with a composition of CuCr0,8Zr0,08 (wt%) were placed on top of the tungsten samples and heated at 1200°C for 30min. The melting CuCrZr flowed into the pores of the tungsten skeleton and formed W/CuCrZr-composites.
Finally the CuCrZr in the samples was precipitation hardened by solution annealing in high vacuum at 970°C for 30min and oil quenching without breaking the vacuum. This was done in a vertical furnace with the sample hanging at a wire that can be melted via the passage of current. The samples were then aged in argon at 480°C for 60min to form precipitates followed by air cooling out of the furnace. Before and after ageing Vickers hardness measurements (294 N force) were carried out to show the effect of precipitation hardening.
For subsequent characterization measurements samples of desired size were prepared. Thermal tests comprised CTE-measurements and the determination of the thermal diffusivity in a laser flash apparatus (LFA 427, Netzsch). For the characterization of mechanical properties E-modulus measurements by resonant frequency analysis (RFA; RFDA system 23, IMCE), 4-point bending tests at room temperature and tensile tests in cooperation with MTU Aero Engines, Germany at RT, 300°C and 550°C were carried out. The samples were inductively heated with 20K/s and tested with 1mm/min. As inputs for the direct mapping FEM procedure SEM images at high resolution were taken. These micrographs were then mapped with the tool OOF developed by NIST, USA [16]. As solver the commercial FEM code ABAQUS v6.7 was used [17]. More detailed information about the underlying direct mapping FEM procedure can be found in [18].

Results and discussion

Synthesis

The composition of used W/wax-mixtures and applied pressures to form tungsten skeletons with the desired porosity are shown in table 1.

mixture	W/wax-ratio [vol.%]	pressure [MPa]	porosity [vol.%]
1	97,3/3,7	600	30
2	60/40	300	50
3	100/0	-	70

Table 1. Used W/wax-mixtures and applied pressures to form tungsten skeletons with the desired porosity

In the case of mixture 1 the small amount of wax served as a pressing agent. On the other hand a too high content of wax results in a diffluence of the green compact during debinding because of insufficient tungsten particle contact. However, to produce dimensionally stable samples the tungsten compacts with the highest porosity of 70 vol.% were fabricated by loose fills of pure tungsten powder in a ceramic ring.
Infiltration experiments in different atmospheres revealed that only in high vacuum it is possible to produce completely infiltrated, dense W/CuCrZr-composites with a homogeneous distribution of the alloying elements. Infiltration in high purity argon led to an incomplete infiltration due to insufficient wetting behaviour of the melted CuCrZr on tungsten. Otherwise an accumulation of the oxygen affine elements Zr and Cr on the sample surface was measured after using hydrogen.
Light microscopy as well as SEM images (with secondary electrons) of the fabricated W/CuCrZr-composites exhibit a fine-grained penetration microstructure nearly without pores. However there is still some inhomogeneity in the tungsten as well as CuCrZr framework visible as shown in figure 1. In both cases this is attributed to agglomerates of tungsten and wax particles in the starting material.

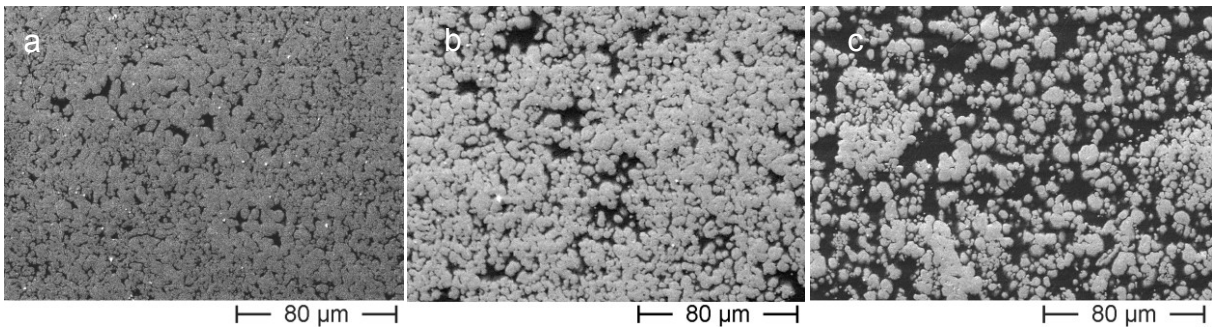

Figure 1. SEM pictures of W/CuCrZr composites with different CuCrZr content (derived from density measurements (a: 30 vol.% CuCrZr; b: 46 vol.% CuCrZr; c: 69 vol.% CuCrZr))

Results of Vickers hardness measurements before and after ageing can be seen in figure 2. It is apparent that with increasing CuCrZr content the hardness increment due to precipitation hardening of the matrix is more pronounced.

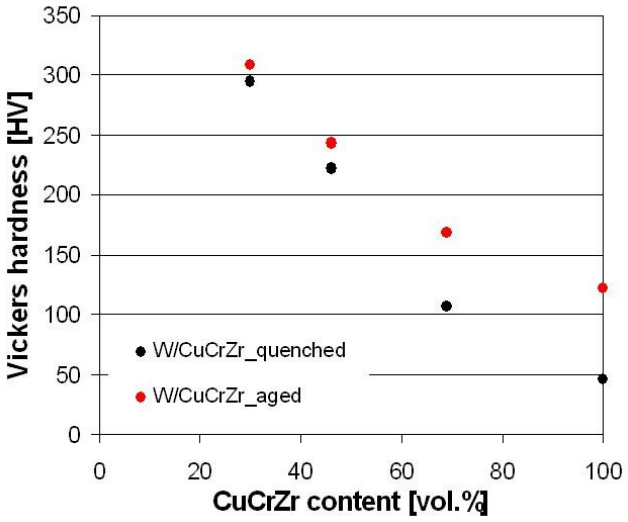

Figure 2. Vickers hardness of W/CuCrZr composites in dependence of CuCrZr content before and after ageing

Characterization

The coefficient of thermal expansion (CTE) versus composition at different temperatures is illustrated in figure 3. With higher CuCrZr content the values of CTE are increasing almost linearly. Furthermore they are rising with temperature.

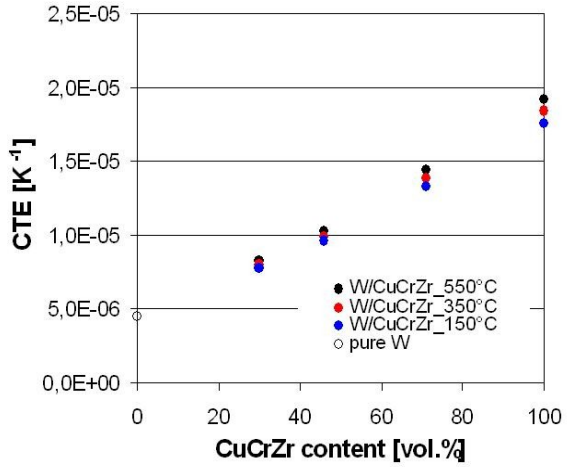

Figure 3. CTE values of W/CuCrZr composites in dependence of CuCrZr content and temperature

The thermal conductivity of the composites was determined by multiplication of the measured thermal diffusivity α, the specific heat capacity $c_{W/CuCrZr}$ and the measured composite density $\rho_{W/CuCrZr}$ (by Archimedes principle). For the calculation of the specific heat capacity the rule of mixture was used:

$$c_{W/CuCrZr} = \frac{1}{\rho_{W/CuCrZr}}(k_W \rho_W c_W + \varphi_{CuCrZr}\rho_{CuCrZr}c_{CuCrZr}) \text{ with } k_W = 1 - \varphi_{CuCrZr}$$

K, ρ and c denote the volume fraction, density and specific heat of the particular material. Data for specific heat values of W und CuCrZr were taken from [19] and [20] resp. In figure 4 the calculated thermal conductivities for the W/CuCrZr-composites are illustrated. The samples with the lowest tungsten content exhibit the highest thermal conductivity (255 W/mK at RT). With increasing tungsten content thermal conductivity decreases. In dependence of temperature thermal conductivity is initially decreasing but beyond 300°C it is constantly rising. This effect is more pronounced at higher CuCrZr contents and is related to the starting coarsening of precipitates in the CuCrZr alloy at elevated temperatures.

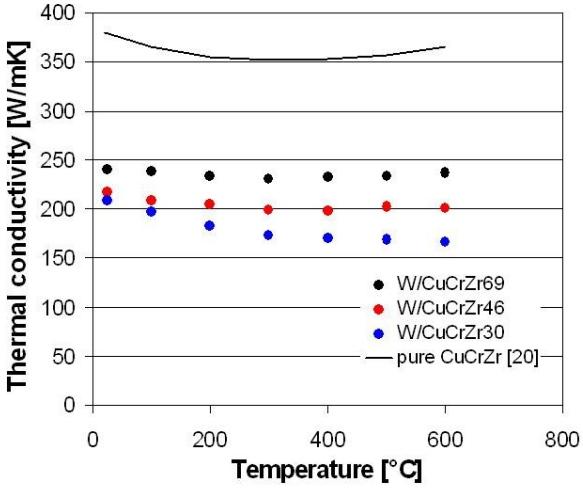

Figure 4. Temperature dependence of thermal conductivity for three different W/CuCrZr composites (CuCrZr content in vol. %).

For the mechanical evaluation of the fabricated W/CuCrZr composites they were initially tested by 4-point bending at room temperature. As shown in figure 5 the determined yield strength $R_{p,0.2}$ is continuously increasing with decreasing CuCrZr content. Compared to literature data of plasma sprayed W/Cu composites the measured values of W/CuCrZr composites are much higher. This is ascribed especially to the positive influence of the hardenable CuCrZr alloy.

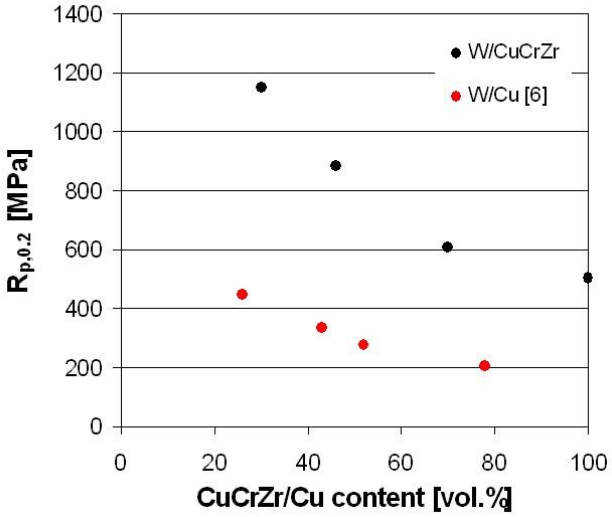

Figure 5. Yield strength $R_{p,0.2}$ of W/CuCrZr composites in dependence of CuCrZr content and compared to literature values for W/Cu composites [6].

Typical stress-strain curves from tensile tests for W/CuCrZr composites with 35 vol.% and 72 vol.% CuCrZr resp. are illustrated in figure 6.

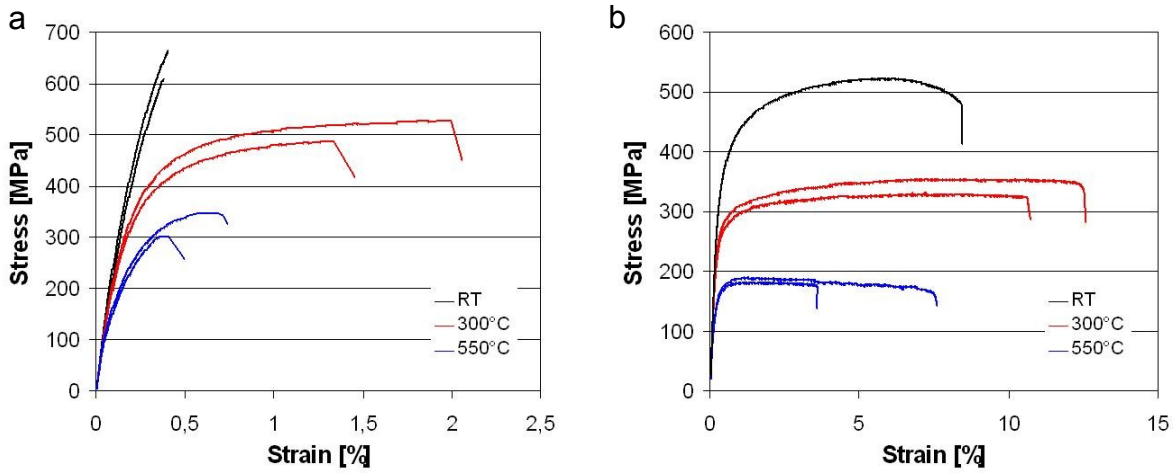

Figure 6. Stress-strain curves from tensile tests for W/CuCrZr35 (a) and W/CuCrZr72 (b) at different test temperatures.

In both cases the ultimate tensile strength R_m is decreasing with an increasing temperature whereby the values for the samples with higher CuCrZr content are generally lower. An interesting trend is observed for the ultimate elongation which reaches the highest values for the mean testing temperature at 300°C as shown in table 2. At that temperature the precipitates in the CuCrZr alloy are still stable and influence the fracture behaviour. At RT and 550°C the total elongation is much lower, especially for high tungsten content. In these cases the fracture behaviour is especially dominated by the tungsten phase. The data in table 2 also indicates a good correlation between the elastic modulus determined from stress-strain curves E_t and measured by RFA E_{RFA} at room temperature.

	Temperature °C	R_m MPa	e_t [%]	E_t [GPa]	E_{RFA} [GPa]
W/CuCrZr35	20	635	0,38	277	281
	300	500	1,66	262	-
	550	320	0,55	254	-
W/CuCrZr72	20	520	8,4	169	176
	300	340	11,5	155	-
	550	185	5,4	130	-

Table 2: Tensile strength R_m, total elongation e_t and E-Modules determined from stress-strain curves E_t and measured by RFA E_{RFA} for two W/CuCrZr composites at different temperatures

FEM-Simulation

In figure 7 the simulated thermal conductivities of two W/CuCrZr composites at different temperatures are plotted in comparison to experimental results. The agreement between simulation and experimental data is quite good considering that simulation material data were taken from literature for both components [21, 22]. The mismatch is decreasing at higher temperatures and rising for increasing volume fraction of CuCrZr with unexpected high values for simulated W/CuCrZr67 at RT (2D limit should always be lower than the real 3D case). This can be ascribed to an overestimation of local conductivity of CuCrZr which should be independently measured in future works.

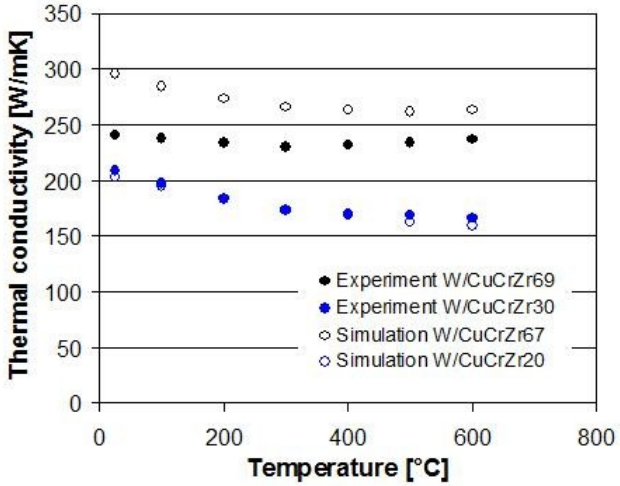

Figure 7. Calculated thermal conductivity for a W/CuCrZr67 and W/CuCrZr20 composite (volume fraction calculated from micrographs used in the simulations) in comparison to experimental data obtained from specimens with a similar morphology (W/CuCrZr69 and W/CuCrZr30; composition derived from density measurements).

The measured and simulated stress-strain curves for the W/CuCrZr composite with a high tungsten content of ~70 vol.% at 300 and 550°C are shown in figure 8. The general trend shows a satisfactory agreement between experimental and numerical results. Again, the mismatch is firstly caused by using literature data instead of single phase stand alone measurements since the performance in the elastoplastic regime (CuCrZr) and brittle failure (W) is extremely sensitive to composition and production parameters. The measured onset of overall specimen failure can furthermore deviate from the individual FEM predictions since it is closely related to the specific morphology and volume fraction. A high scatter for the ultimate total strain was already observed in [18] for a high content of CuCrZr. On the other hand, the strong gap between 550 and 300 °C is well reproduced by the simulations.

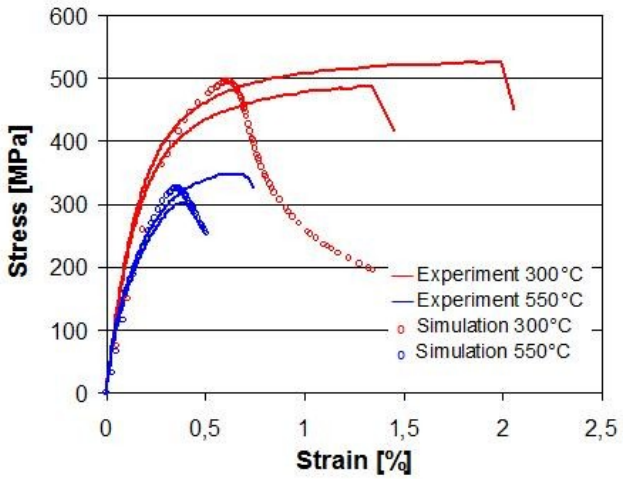

Figure 8. Comparison between the experimental (W/CuCrZr35) and numerical (W/CuCrZr20) tensile stress-strain data of a tungsten-rich W/CuCrZr composite.

W/CuCrZr gradient structures

A typical W/CuCrZr gradient structure built up of three layers (70, 54 and 30 vol.% CuCrZr resp.) is shown in figure 9a. The corresponding interfaces between the individual layers in figure 9b and c reveal a relative good bonding. Except some small pores the porous graded tungsten skeleton was completely infiltrated with CuCrZr.

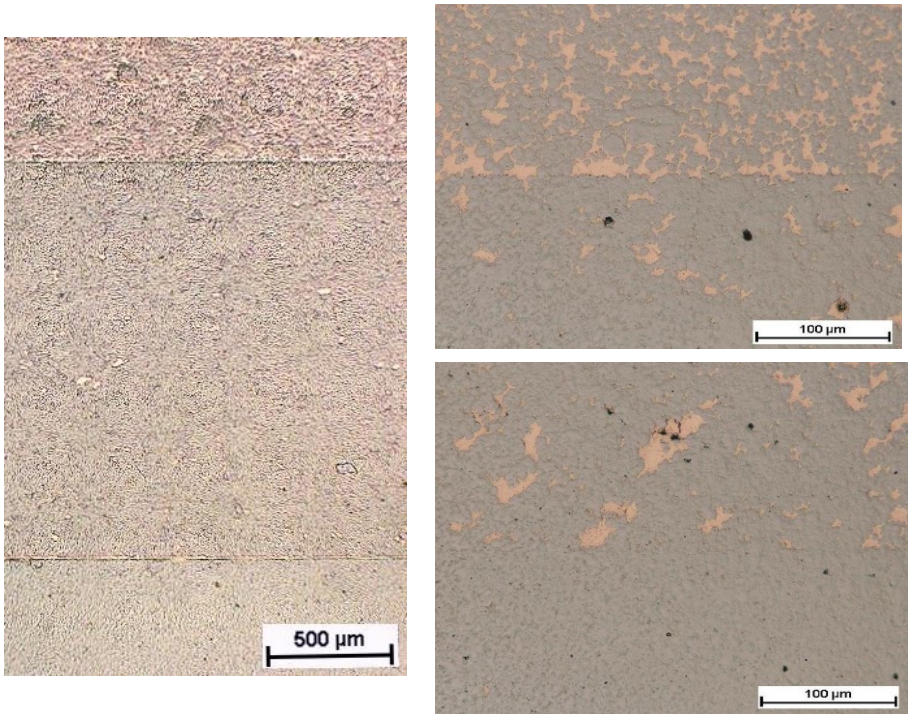

Figure 9. Typical W/CuCrZr gradient structure built up of three layers (70, 46 and 30 vol.% CuCrZr resp.) (a) with corresponding interfaces W/CuCrZr70-W/CuCrZr46 (b) and W/CuCrZr46-W/CuCrZr30 (c).

Conclusion

In the present study it was shown that dense W/CuCrZr composites as well as layered FGMs in a composition range between 30 and 70 vol.% tungsten can be produced by forming a tungsten skeleton with open pores and subsequent CuCrZr infiltration. The fabricated samples showed a fine-grained penetration microstructure with nearly no pores. Furthermore the utilization of the hardenable CuCrZr alloy had a strong impact on the achieved strength of the composites. The calculated data of W/CuCrZr composites by direct mapping FEM was in general in good agreement with experimental values. Additional tuning is required to further improve the alignment with experimental data but the results shown are very promising in view of the future optimization of W/CuCrZr gradient structures.
The production of complete W/CuCrZr PFCs together with an extensive evaluation in a heat-flux test facility is planned.

Acknowledgements

This work was funded by Deutsche Forschungsgemeinschaft.

References

[1] Y. Itoh, M. Takahashi, H. Takano; Fusion Engineering and Design 31 (1996) 279
[2] C.-C. Ge, J.-T. Li, Z.-J. Zhou, W.-B. Cao, W.-P. Shen, M.-X. Wang, N.-M. Zhang, X. Liu, Z.-Y. Xu; Journal of Nuclear Materials 283-287 (2000) 1116
[3] Z.-J. Zhou, S.-X. Song, J. Du, Z.-H. Zhong, C.-C. Ge; Journal of Nuclear Materials 363–365 (2007) 1309
[4] W. Schatt, K.-P. Wieters, B. Kieback (Eds.): Pulvermetallurgie / Technologien und Werkstoffe, Springer-Verlag, Berlin, Heidelberg (2007)
[5] B. Kieback, A. Neubrand, H. Riedel; Materials Science and Engineering A362 (2003) 81
[6] G. Pintsuk, S.E. Brünings, J.-E. Döring, J. Linke, I. Smid, L. Xue; Fusion Engineering and Design 66-68 (2003) 237
[7] U.Birth, M.Joensson, B.Kieback; Proceedings of the Powder Metallurgy World Congress, Granada, Spain (1998) 375
[8] R. Jedamzik, A. Neubrand, J. Rödel; Journal of Materials Science 35 (2000) 477
[9] D. Jankovic Ilic, J. Fiscina, C. J. R. Gonzalez-Oliver, N. Ilic, F. Mücklich; Journal of Materials Science 43 (2008) 6777
[10] R.M. German; Metallurgical Transactions A, Volume 24A (1993) 1745
[11] M. Joensson, U. Birth, J. Schreiber, S. Fischer, B. Kieback; Proceedings of the 4th International Conference on Composites Engineering, Hawaii, USA (1997) 495
[12] U. Birth, M. Joensson, B. Kieback; Proceedings of the 5th International Symposium on Functionally Graded Materials, Dresden, Germany (1998) 766
[13] M.M. Gasik; Computational Materials Science 13 (1998) 42
[14] B.N. Singh, D.J. Edwards, M. Eldrup, P. Toft; Journal of Nuclear Materials 249 (1997) 1
[15] N. Chawla, B.V. Patel, M. Koopman, K.K. Chawla, R. Saha, B.R. Patterson, E.R. Fuller, S.A. Langer; Materials Characterization 49 (2003) 395
[16] S.A. Langer, E.R. Fuller, W.C. Carter, Computing in Science and Engineering 3 (2001) 15
[17] ABAQUS User's Manual 6.8, Dassault systems, Providence (2008)
[18] A. Zivelonghi, A. Brendel, S. Lindig, S. Nawka, B. Kieback, J.H. You; Journal of Nuclear Materials, accepted
[19] VDI-Wärmeatlas, Springer-Verlag, Berlin (1997)
[20] ITER Material Properties Handbook, ITER Document No. S 74 MA 2
[21] ITER Material Properties Handbook, ITER Document No. S 74 RE 1
[22] ITER Material Properties Handbook, ITER Document No. G74 MA16